Radiology

Optimization of Multiplanar Reformations from Isotropic Data Sets Acquired with 16–Detector Row Helical CT Scanner[1]

Tracy A. Jaffe, MD
Rendon C. Nelson, MD
G. Allan Johnson, PhD
Ellie R. Lee, MD
Terry T. Yoshizumi, PhD
Carolyn R. Lowry, BSRT (R)(CT)
Anthony B. Bullard, MD
David M. DeLong, PhD
Erik K. Paulson, MD

Institutional review board approval and waiver of consent were obtained for the patient component of this retrospective HIPAA-compliant study. By using an anthropomorphic phantom and metal oxide semiconductor field effect transistor detectors, radiation dose was determined for one eight–detector row and two 16–detector row computed tomographic (CT) protocols. A custom phantom was scanned by using the three protocols to identify isotropy. Contrast-to-noise ratios (CNRs) were determined for the same protocols by using a third phantom. Seven patients had undergone isotropic 16–detector row CT of the abdomen and pelvis. Anonymized coronal reformations at various thicknesses were ranked qualitatively by three radiologists. Effective dose equivalents were similar for the eight– and 16–detector row protocols. When transverse and coronal reformations of data acquired in the custom phantom were compared, coronal reformations obtained with the 16–detector row and 0.625-mm section thickness protocol were found to be nearly identical to the transverse image for all sets of line pairs. CNRs were consistently highest on 5-mm-thick coronal reformations (CNR range, 1.2–3.3). For qualitative assessment, 2- and 3-mm-thick coronal reformations were consistently preferred.

[1] From the Department of Radiology, Duke University Medical Center, Box 3808, Durham, NC 27710. Received March 10, 2005; revision requested April 29; revision received June 22; accepted June 27; final version accepted July 8.

Since the introduction of computed tomography (CT) scanners in the 1980s, rapid technologic advances have altered the application of this modality in clinical use. With the introduction of single-section helical scanners in the early 1990s, followed by the introduction of multi–detector row helical scanners in the late 1990s, there has been a trend toward the acquisition of more sections per gantry rotation. The use of multi–detector row CT scanners enables an increase in scanning speed and a subsequent reduction in scanning time, increase in scanned volume, and increase in spatial resolution along the z-axis (1). These advances have dramatically changed imaging of the abdomen and pelvis because large areas of anatomic interest can now be scanned with thin sections during a single comfortable breath hold. Application of these technological changes requires revision of scanning protocols according to the number of sections acquired per gantry rotation, with attention to maintaining radiation dose and image quality—particularly in terms of image noise (2,3). There is a substantial body of work in the literature regarding the optimization of CT parameters and body imaging protocols for four– and eight–detector row scanners (1–8). Most of the optimization studies with 16–detector row scanners have focused on cardiac imaging. Similar efforts regarding the use of 16–detector row CT scanners in abdominal and pelvic imaging are important.

Advances in Knowledge

- It is possible to obtain isotropic data sets without an increase in radiation dose or loss of CNR at 16–detector row CT.
- Multiplanar reformations of images of the abdomen and pelvis performed with data from isotropic CT data sets have image quality that rivals that of transverse images.
- There is no benefit to overlapping reconstruction of isotropic data sets.

The obvious advantages of 16–detector row CT scanners include the fact that they enable a marked decrease in scanning time and improvement in image quality compared with the scanning time and image quality achievable with previous scanners. With the use of thinner section widths we have achieved greater spatial resolution and a reduction in partial volume averaging. Perhaps most important, this detector configuration enables submillimeter section acquisition, which in turn yields isotropic voxels (ie, voxels that have the same measurements in all three axes). This isotropy enables the generation of multiplanar reformations with similar image quality to that of transverse images without complicated interpolation steps. Thus, the purpose of our study was to determine the optimal parameters for multiplanar reformations of 16–detector row CT data with isotropic voxels.

Materials and Methods

Phantom Study

All data were acquired with a 16–detector row CT scanner (Lightspeed 16; GE Healthcare, Milwaukee, Wis). We selected several protocols for comparison by using both eight– and 16–detector row configurations. The definition of pitch used in this study was the classic definition of beam pitch: the true longitudinal distance covered during a single gantry rotation divided by the beam collimation width (the product of the number of detector rows and the minimum section thickness). The eight–detector row protocol chosen for this study reflected the protocol in use during our current daily practice—a protocol for which we have previously reported our optimization results (4), which indicated that a detector configuration of 8×1.25 mm (where 8 is the number of detector rows and 1.25 mm is the section thickness) with a pitch of 1.675 is optimal. The 16–detector row configurations were as follows: 16×0.625 mm with a pitch of 1.750 (a protocol for routine imaging) and 16×1.25 mm with a pitch of 1.375 (a protocol for CT angiography). The gantry rotation time used for this study was 0.5 second (Table 1).

The 16×0.625 mm protocol with a pitch of 1.750 was designed to maintain a constant radiation dose compared with the dose from an eight–detector row CT scanner. Radiation doses were calculated prospectively by using a proprietary dose-simulator program (Lightspeed Protocol Simulator, version 4.3; GE Healthcare). Peak voltage was kept at 140 kVp, and tube current per rotation was varied from 270 to 360 mA to maintain constant noise. An anthropomorphic phantom (Computerized Imaging Reference System, Norfolk, Va) with imbedded metal oxide semiconductor field effect transistor, or MOSFET, detectors (Thomson-Nielson, Ottawa, Ontario, Canada) was used to verify the true radiation dose levels for each protocol; the phantom was scanned with each protocol a total of four times and the MOSFET detectors were used to calibrate the effective dose equivalent for each variation in protocol (T.T.Y.).

A second custom phantom designed and built at our institution was then scanned with the three protocols so that we could evaluate spatial resolution. This phantom contained high-contrast funk bars that measured modulation

Published online
10.1148/radiol.2381050404

Radiology 2006; 238:292–299

Abbreviations:
CNR = contrast-to-noise ratio
MTF = modulation transfer function
ROI = region of interest

Author contributions:
Guarantor of integrity of entire study, T.A.J.; study concepts/study design or data acquisition or data analysis/interpretation, all authors; manuscript drafting or manuscript revision for important intellectual content, all authors; approval of final version of submitted manuscript, all authors; literature research, T.A.J., G.A.J., D.M.D.; clinical studies, T.A.J., E.R.L., T.T.Y., C.R.L., A.B.B.; experimental studies, T.A.J., R.C.N., G.A.J., T.T.Y., C.R.L., A.B.B.; statistical analysis, T.A.J., R.C.N., G.A.J., T.T.Y., D.M.D.; and manuscript editing, T.A.J., R.C.N., D.M.D., E.K.P.

Address correspondence to T.A.J. (e-mail: *jaffe002@mc.duke.edu*).

R.C.N. is a consultant for GE Healthcare.

transfer functions (MTFs) in both the transverse (acquired) and coronal (reformatted) planes (Fig 1). One bar was placed parallel to the plane of acquisition (the *x-y* plane), and the other was placed parallel to the z-axis. Both sets of funk bars contained six patterns of four bars of varying thickness that were arranged in groups ranging from 1.6 to 9.8 line pairs per centimeter.

To evaluate spatial resolution, we scanned the custom phantom described above by using one eight–detector row configuration (8 × 1.25 mm with a pitch of 1.675) and three 16–detector row configurations (16 × 1.25 mm with a pitch of 1.375 and 16 × 0.625 mm with a pitch of 1.750 and two variations in reconstruction interval: 0.5 mm [overlapping] and 0.625 mm [nonoverlapping]). Again, the tube current and table speed varied with each protocol (Table 2). The four protocols used in this study were designed with variations to enable specific protocol comparisons: Protocol A (detector configuration, 8 × 1.25 mm) was considered to be a baseline protocol; protocol B (detector configuration, 16 × 1.25 mm) was designed to reduce scanning time while keeping spatial resolution along the z-axis, noise, and dose fixed with regard to those of the baseline protocol; and protocols C and D (detector configuration, 16 × 0.625 mm) were designed to increase resolution along the z-axis while keeping scanning time and noise fixed relative to those of the baseline protocol (although the dose was expected to increase). Protocols C and D consisted of the same acquisition parameters but were different in terms of their reconstruction parameters. Protocols C (reconstruction thickness, 0.625 mm at 0.5-mm intervals [overlapping]) and D (reconstruction thickness and interval [nonoverlapping], 0.625 mm) were designed so that we could determine the effect of overlapping reconstruction of isotropic voxels. An MTF was applied to each reformation; the MTFs were then directly compared. This comparison was performed by measuring the amplitude of each segment of the MTF (G.A.J.).

To evaluate contrast-to-noise ratios (CNRs), a third phantom (Catphan; Phantom Laboratory, Salem, NY) (Fig 2) was scanned by using the same four protocols used for scanning the custom phantom. The Catphan phantom was chosen for its configuration of low- and high-density internal materials. Coronal reformations of these scans were performed at 1-, 2-, 3-, 4-, and 5-mm thicknesses for each protocol (T.T.Y.).

Table 1

Multi–Detector Row CT Parameters for Radiation Dose Determination

Detector Configuration	Pitch	Table Speed*	Rotation Time (sec)	Peak Voltage (kVp)	Tube Current (mA)
8 × 1.25 mm	1.675	16.75	0.5	140	270
16 × 1.25 mm	1.375	27.50	0.5	140	360
16 × 0.625 mm	1.750	17.50	0.5	140	280

* In millimeters per rotation.

Figure 1

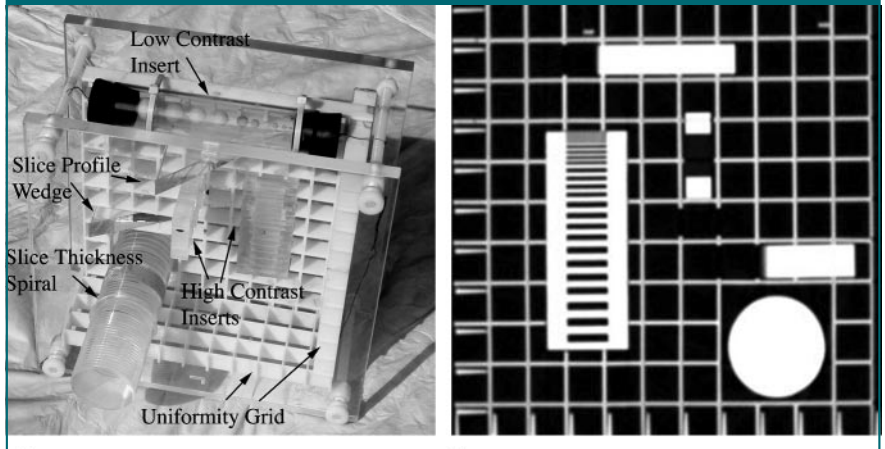

a. b.

Figure 1: **(a)** High-contrast phantom used to evaluate quality of z-axis reformations by using MTFs. High-contrast inserts are placed at 90° to each other. **(b)** Representative transverse CT scan of high-contrast phantom acquired at 140 kVp.

Table 2

Multi–Detector Row CT Parameters for Scanning of Spatial Resolution Phantom

Detector Configuration	Pitch	Table Speed*	Reconstruction Thickness (mm)	Reconstruction Interval (mm)	Tube Current (mA)
8 × 1.25 mm	1.675	16.75	1.25	0.5	100
16 × 1.25 mm	1.375	27.50	1.25	0.5	90
16 × 0.625 mm	1.750	17.50	0.625	0.5	225
16 × 0.625 mm	1.750	17.50	0.625	0.625	225

* In millimeters per rotation.

Patient Study

The retrospective patient arm of the study was approved by the institutional review board with a waiver of informed consent and was compliant with the Health Insurance Portability and Accountability Act. To determine the qualitative assessment of coronal reformation thickness, we included in our study seven consecutive patients who underwent CT scanning in June 2003. There were three women and four men with a mean age of 55 years (age range, 42–68 years) and a clinical complaint of abdominal pain. CT scanning of the abdomen and pelvis was performed by using the protocol that involved a detector configuration of 16 × 0.625 mm, a pitch of 1.750, and a reconstruction thickness and interval of 0.625 mm (protocol D).

These images were reformatted in the coronal plane at section thicknesses of 1, 2, 3, 4, and 5 mm by using the Xtreme reconstruction package (GE Healthcare), a reconstruction processor on the operator's console. This reconstruction engine is comprised of dual 2.66-GHz Xenon processors (Intel, Santa Clara, Calif) and is able to generate 6–10 images per second. Total reconstruction time was approximately 2–3 minutes; reconstruction were performed by the technologist (C.R.L.). Three readers (A.B.B., T.A.J., and R.C.N.) with 3 years of residency training and 3 and 15 years of abdominal imaging experience, respectively, evaluated these images in a side-by-side fashion for qualitative appearance. Images were anonymized in accordance with Health Insurance Portability and Accountability Act regulations.

The readers were unaware of the reformation section thickness for each image because the images were arranged in random order. The readers were asked to independently rank the five reformatted images in order of diagnostic preference (not image noise preference) by using a ranking system in which a score of 1 indicated the best image and a score of 5 indicated the worst image. Readers were given verbal instructions as to our criteria for diagnostic preference, which included how well small structures could be identified and whether or not there was loss of information on the scan. Given that no strict imaging criteria were used, diagnostic preference was a subjective ranking.

Figure 2

Figure 2: Catphan phantom. This phantom contains separate compartments that are used for evaluation of CNR.

Figure 3

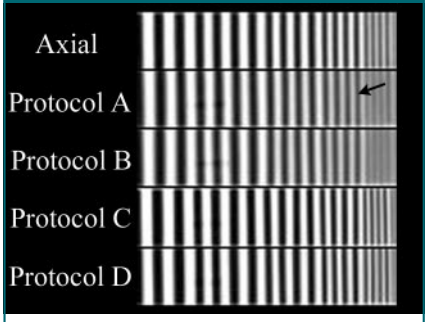

Figure 3: Transverse and z-axis reformations of CT data acquired in high contrast phantom. The transverse scan at the top serves as the reference. The use of protocols A and B yielded diminished resolution relative to that yielded by standard transverse scanning and protocols C and D. Note the blur in the edges of all the bar patterns and the reduced gray-scale differentiation in the second-to-last pattern (arrow).

Data and Statistical Analyses

Data were analyzed for each phantom separately. Data from the radiation dose measurements are reported in millisieverts, and a standard deviation was generated for each protocol. Statistical analysis was performed for heterogeneity of variances, and the mean values were evaluated by using a two-way analysis of variance that included detector configuration and section thickness.

Images of the high-contrast spatial resolution custom phantom were analyzed by comparing a true transverse image with a z-axis (longitudinal) reformation created at a workstation (Vitrea 2, version 3.3; Vital Images, Minneapolis, Minn). An MTF was applied to both the transverse image and to each reformation; the MTFs were then directly compared. This comparison was performed visually, as well as by measuring the amplitude of each segment of the MTF (G.A.J.). The CNRs were examined by means of a two-way analysis of variance that included detector configuration and reformation thickness.

Data from the Catphan phantom were evaluated for low-contrast detectability by using CNRs. This was accomplished by using a 51-mm^2 standard round region of interest (ROI) that was applied to both the phantom and the background on two similar regions on the five coronal reformations acquired with each protocol. The ROI was applied by one author (A.B.B.) on all images. CNRs were then calculated as follows: $(ROI_M - ROI_B)/SD_B$, where ROI_M and ROI_B are CT numbers measured in the ROIs of the high-attenuating soft tissue and the air or background, respectively, and SD_B represents the standard deviation of the background noise. Standard deviations were calculated; they were then compared by means of the maximum ratio. Mean CNRs were analyzed by using the Student range test.

Data from the qualitative assessment of patient images was analyzed by determining the mean and standard deviation for each rank. The reader-averaged preference ranking data were analyzed by using the Friedman test, followed by a permutation range test to control for multiple comparisons (9, 10). The permutation range test was based on 100 000 Monte Carlo replicates for the permutation distribution. We used statistical software (SAS, version 8.2; SAS Institute, Cary, NC) for these analyses. *P* values less than .05 were considered to indicate statistically significant differences.

Figure 4

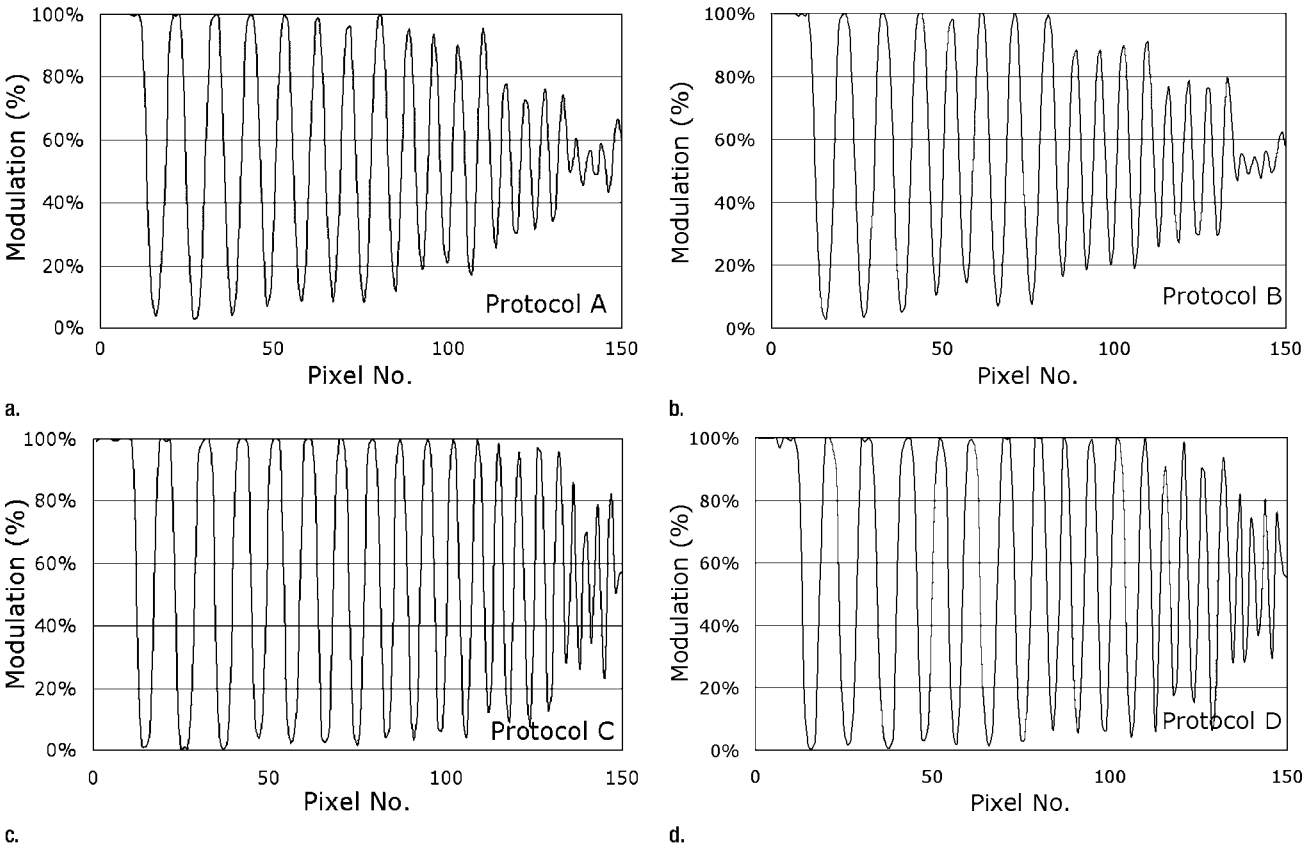

Figure 4: MTFs for the four CT protocols used to image the high-contrast phantom. **(a)** Protocol A (8 × 1.25 mm, 16.75 mm per rotation, pitch of 1.675). **(b)** Protocol B (16 × 1.25 mm, 27.50 mm per rotation, pitch of 1.375). **(c)** Protocol C (16 × 0.625 mm, 17.50 mm per rotation, pitch of 1.750, reconstruction thickness of 0.625 mm at 0.5-mm intervals). **(d)** Protocol D (16 × 0.625 mm at 17.50 mm per rotation, pitch of 1.750, reconstruction thickness of 0.625 mm at 0.625-mm intervals). Note the loss of modulation depth (the clear distinction between white and black) for protocols A and B at the higher numbers of line pairs per centimeter. The 16 × 0.625-mm protocols have comparable modulation profiles.

Results

The radiation doses for the three main protocols (a detector configuration of 8 × 1.25 mm and a pitch of 1.675, a detector configuration of 16 × 1.25 mm and a pitch 1.375, and a detector configuration of 16 × 0.625 mm and a pitch of 1.750) were similar and not substantially different from that predicted by the simulator. The mean dose for the 8 × 1.25-mm protocol was 20.1 mSv ± 0.8 (standard deviation) (range, 18.9–20.8 mSv), the mean dose for the 16 × 1.25-mm protocol was 20.6 mSv ± 0.48 (range, 19.9–21.0 mSv), and the mean dose for the 16 × 0.625-mm protocol was 21.4 mSv ± 0.07 (range, 21.3–21.5 mSv). The effective dose equivalent values were examined by means of a two-way analysis of variance that included detector configuration and section thickness, and this analysis revealed that neither variable was significant at the .05 level ($P = .052$ for configuration and $P = .56$ for section thickness).

Evaluation of the images of the high-contrast inserts that were reformatted for coronal display revealed a decrease in spatial resolution compared with the spatial resolution of the transverse image for protocols A and B (8 × 1.25 mm and 16 × 1.25 mm). This decrease in spatial resolution was evidenced by a blur in the edges of all bar patterns and reduced gray-scale differentiation in the second-to-last pattern (Fig 3). The MTFs for the two 16 × 0.625-mm protocols were superior to those for the 16 × 1.25-mm and 8 × 1.25-mm protocols. The spatial resolution was markedly diminished in protocol B (16 × 1.25 mm); at 9.8 line pairs per centimeter, the peak-to-peak modulation for protocol B was less than 10%. The peak-to-peak modulation at 4.9 line pairs per centimeter for protocol B was approximately 60%, while the modulation for the transverse phantom and protocol C (16 × 0.625 mm) was greater than 90% (Fig 4). This demonstrates that protocol C (and, by extension, protocol D) was comparable with standard transverse scanning; the spatial resolution was isotropic. There was no meaningful difference in the MTFs between protocol C and D. That is, our data indicate that when

one is acquiring isotropic voxel data sets, there is no benefit to overlapping the section reconstruction.

We found that the CNRs for the 5-mm reformation thickness were the highest for each protocol (Table 3). The CNRs were examined by means of a two-way analysis of variance that included detector configuration and reformation thickness. The effect of reformation thickness was significant ($P < .01$). Modeling the effect of reformation thickness as a linear function was found to be adequate because the additional nonlinear effects of thickness were not significant ($P = .26$). Essentially, the thicker the reformatted section, the higher the CNR because the voxels have a larger z-axis dimension. That is, even though the coronal images were reconstructed from an isotropic transverse data set, they were displayed with nonisotropic voxels to diminish the noise and reduce the radiation dose.

With respect to qualitative analysis, readers consistently preferred the 2- and 3-mm coronal reformations for interpretive purposes (Fig 5). The Friedman test for preference differences among the different reformation thicknesses yielded a significant value ($P < .01$). Examination of the pairwise differences in preference between reformation thicknesses by means of the range distribution at a .05 significance level revealed that the 3-mm thickness was preferred to the 1- and 5-mm thicknesses and that the 2-mm thickness was preferred to the 1-mm thickness. The 4- and 5-mm-thick reformations were generally considered to be too smooth. Conversely, the 1-mm-thick sections were too noisy and were therefore least preferred (Fig 6).

Table 3

CNR Comparison: Low-Contrast Detectability with Each CT Protocol

Protocol	Detector Configuration	Pitch	Table Speed*	Reformation Thickness (mm)	CNR
A	8 × 1.25 mm	1.675	16.75	1	1.5
				2	2.1
				3	2.4
				4	2.4
				5	2.8
B	16 × 1.25 mm	1.375	27.50	1	1.7
				2	2.0
				3	2.6
				4	2.9
				5	3.3
C	16 × 0.625 mm	1.750	17.50	1	1.4
				2	1.3
				3	1.6
				4	2.0
				5	2.2
D	16 × 0.625 mm	1.750	17.50	1	1.7
				2	2.0
				3	2.0
				4	1.2
				5	2.5

* In millimeters per rotation.

Figure 5

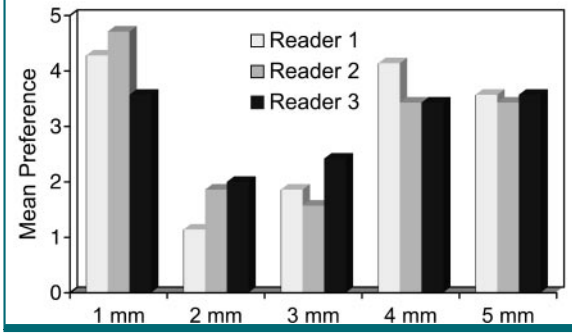

Figure 5: Bar graph shows mean preference ratings for coronal images from isotropic data sets reformatted at 1-, 2-, 3-, 4-, and 5-mm thicknesses (horizontal axis). Three different readers rated the images according to diagnostic preference from 1 (best) to 5 (worst).

Discussion

One of the most heralded advantages of multi–detector row CT scanning is the increase in scanning speed. Imaging of the entire abdomen and pelvis can now be performed during a single short breath hold. With each advance in detector configuration technology, scanning times have continued to decrease (4,6). Because there are few advantages to even faster scanning of the abdomen and pelvis, further advances in multi–detector row CT technology have come in the form of an improvement in image quality. The additional detector rows enable the acquisition of thinner sections, which in turn leads to improved resolution in the z-axis (longitudinal axis), with the acquisition of isotropic data sets as the goal. These data sets can then be manipulated into high-quality multiplanar reformations. To our knowledge, the optimal scanning parameters for the multiplanar reformations created from 16–detector row CT data have not been previously delineated.

Previous investigators have proved that it is possible to increase the quality of multi–detector row CT scans by adding detector rows without a substantial increase in radiation (4). Our data continue to support this theory: We found that there is no statistically significant increase in effective dose equivalent when transitioning from an eight– to a 16–detector row CT protocol. This is

Figure 6

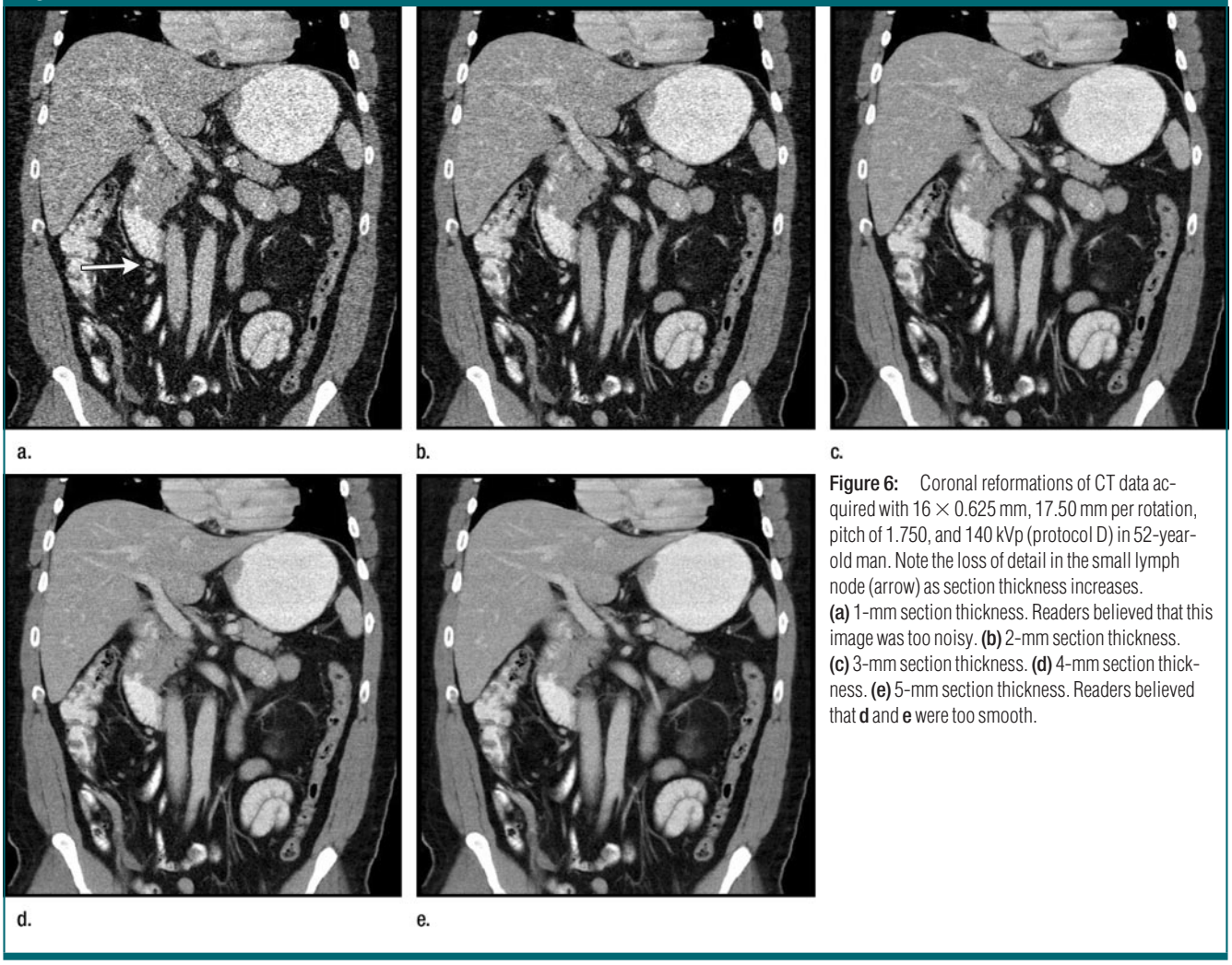

Figure 6: Coronal reformations of CT data acquired with 16 × 0.625 mm, 17.50 mm per rotation, pitch of 1.750, and 140 kVp (protocol D) in 52-year-old man. Note the loss of detail in the small lymph node (arrow) as section thickness increases. **(a)** 1-mm section thickness. Readers believed that this image was too noisy. **(b)** 2-mm section thickness. **(c)** 3-mm section thickness. **(d)** 4-mm section thickness. **(e)** 5-mm section thickness. Readers believed that **d** and **e** were too smooth.

true if the image reconstruction thickness and the noise level are the same. If thinner sections are reconstructed in a comparison of eight– and 16–detector row CT protocols (eg, 1.25 vs 0.625 mm), the dose at 16–detector row CT will increase, assuming similar noise levels. This phenomenon is partially offset by the use of faster table speeds with the 16–detector row CT scanner (eg, 16.75 mm per rotation with the eight–detector row CT scanner vs 17.50 mm per rotation with the 16–detector row scanner), but the radiation dose difference is not substantial.

Our data demonstrated that obtaining isotropic data sets is now possible with 16–detector row CT. Just as was previously seen with the comparison between four– and eight–detector row CT (4), z-axis resolution dramatically improved with the expansion to 16 detector rows; the thinnest section width was submillimeter (0.625 mm). Improvement in z-axis resolution was evident through both visual inspection and the comparison of MTFs. Furthermore, there was no appreciable difference in z-axis resolution with overlapping reconstruction of isotropic voxels.

It is interesting to note that, despite the fact that the 5-mm coronal images had the highest CNR, the readers consistently preferred the images obtained at reformation thicknesses of 2 or 3 mm. The readers believed that the 1-mm-thick images contained too much noise and that the 4- and 5-mm-thick sections depicted less detail in subcentimeter structures such as small lymph nodes and vessels. This loss of detail was in large part the reason for the preference of intermediate section thicknesses; at such thicknesses (2 or 3 mm), the information obtained from the greater degree of anatomic detail outweighed the relative increase in noise compared with the noise in thicker sections. The fact that image quality is not necessarily affected by image noise has been corroborated by results of several other studies (7).

The ability to create isotropic multiplanar reformations has many applications. Multiplanar reformations can convey complex anatomic and pathologic information, and the choice of de-

tector configuration and, ultimately, beam collimation directly affects the quality of image postprocessing (7). Early use of multiplanar reformations was restricted by limited z-axis resolution and longer acquisition times. These reformations were degraded by motion, which resulted in stair-step artifacts (8). The use of submillimeter isotropic data sets has proved advantageous in cardiac, pulmonary, and musculoskeletal imaging because such data facilitate the delineation of coronary arteries and bypass grafts, pulmonary disease, and complex skeletal fractures (11–17). The use of isotropic multiplanar reformations in abdominal imaging may also enhance the current practice of multi–detector row CT urography (18–20). The coronal reformations obtained from isotropic data sets have already proved to increase confidence in the evaluation of the gastrointestinal tract, especially in patients suspected of having appendicitis or small-bowel obstruction, and are being used in practice for a number of clinical applications (16,21,22).

There were limitations to our study. Although this study was designed to evaluate optimization of isotropic multiplanar reformations, it did not address the question of whether these reformations are clinically superior to nonisotropic multiplanar reformations. Furthermore, our study did not involve the assessment of sagittal, oblique, or curved multiplanar reformations.

In conclusion, our data support the idea that with 16–detector row CT, isotropic data sets are easily obtainable, with no increase in the radiation dose or loss in CNR when compared with the dose and CNR at eight–detector row CT. Furthermore, these isotropic data sets can be used to create multiplanar reformations with optimal z-axis resolution and wide clinical applications. The ideal scanning parameters, which are now used routinely in our practice, include use of the narrowest beam collimation at a fast pitch of 1.500–1.750. Coronal reformations should be obtained by using 2–3-mm section thicknesses for best diagnostic quality. It is not necessary to perform overlapping reconstructions of isotropic data sets.

References

1. Prokop M. Multislice CT angiography. Eur J Radiol 2000;36:86–96.
2. Yoshizumi TT, Nelson RC. Radiation issues with multidetector row helical CT. Crit Rev Comput Tomogr 2003;44:95–117.
3. Thornton FJ, Paulson EK, Yoshizumi TT, Frush DF, Nelson RC. Single versus multi–detector row CT: comparison of radiation doses and dose profiles. Acad Radiol 2003; 10:379–385.
4. Gupta AK, Nelson RC, Johnson GA, Paulson EK, DeLong DM, Yoshizumi TT. Optimization of eight-element multi–detector row helical CT technology for evaluation of the abdomen. Radiology 2003;227:739–745.
5. Hu H, He HD, Foley WD, Fox SH. Four multidetector-row helical CT: image quality and volume speed coverage. Radiology 2000; 215:55–62.
6. Killius JS, Nelson RC. Logistical advantages of four-section helical CT in the abdomen and pelvis. Abdom Imaging 2000;25:643–650.
7. Hong C, Bruening R, Schoepf UJ, Bae KT, Reiser MF. Multiplanar reformat display technique in abdominal multidetector row CT imaging. Clin Imaging 2003;27:119–123.
8. Fleischmann D, Rubin GD, Paik DS, et al. Stair-step artifacts with single versus multiple detector-row helical CT. Radiology 2000; 216:185–196.
9. Friedman M. The use of ranks to avoid the assumption of normality implicit in the analysis of variance. J Am Stat Assoc 1937;32: 675–699.
10. Sen PK. On a class of aligned rank order tests in two-way layouts. Ann Math Stat 1968;39:1115–1124.
11. Dewey M, Lembcke A, Enzweiler C, Hamm B, Rogalla P. Isotropic half-millimeter angiography of coronary artery bypass grafts with 16-slice computed tomography. Ann Thorac Surg 2004;77:800–804.
12. Honda O, Johkoh T, Yamamoto S, et al. Comparison of quality of multiplanar reconstructions and direct coronal multidetector CT scans of the lungs. AJR Am J Roentgenol 2002;179:875–879.
13. Kozuka T, Tomiyama N, Johkoh T, et al. Coronal multiplanar reconstruction view from isotropic voxel data sets obtained with multidetector-row CT: assessment of detection and size of mediastinal and hilar lymph nodes. Radiat Med 2003;21:23–27.
14. Rydberg J, Buckwalter KA, Caldemeyer KS, et al. Multisection CT: scanning techniques and clinical applications. RadioGraphics 2000;20:1787–1806.
15. Kopp AF, Küttner A, Trabold T, Heuschmid M, Schröer S, Claussen CD. Multislice CT in cardiac and coronary angiography. Br J Radiol 2004;77(spec no 1):S87–S97.
16. Rydberg J, Sandrasegaran K, Lall CG, Hameed TA, Hawes DR, Kopecky KK. Routine isotropic scanning of the abdomen and pelvis using a 40-channel CT scanner: value of reformatted coronal and sagittal images in showing pathology (abstr). In: Radiological Society of North America scientific assembly and annual meeting program. Oak Brook, Ill: Radiological Society of North America, 2004; 778.
17. Philipp MO, Kubin K, Mang T, Hormann M, Metz VM. Three-dimensional volume rendering of multidetector-row CT data: applicable for emergency radiology. Eur J Radiol 2003;48:33–38.
18. Noroozian M, Cohan RH, Caoili EM, Cowan NC, Ellis JH. Multislice CT urography: state of the art. Br J Radiol 2004;77(spec no 1): S74–S86.
19. Rostogi NV, Sahani DV, Lembcke A, McGowan JJ, Gervais DA, Saini S. State-of-the-art imaging of the kidneys and urinary tract with 16 slice MDCT (abstr). In: Radiological Society of North America scientific assembly and annual meeting program. Oak Brook, Ill: Radiological Society of North America, 2004; 724.
20. Lee HJ, Kim SH, Lee KH, et al. New paradigm of urinary tract imaging: coronal display from isotropic 16 multislice CT acquisition (abstr). In: Radiological Society of North America scientific assembly and annual meeting program. Oak Brook, Ill: Radiological Society of North America, 2004; 724.
21. Paulson EK, Harris JP, Jaffe TA, Haugan PA, Nelson RC. Coronal reformations from isotropic voxels using 16 slice MDCT: value in the diagnosis of acute appendicitis. Radiology 2005;235:879–885.
22. Jaffe TA, Martin LC, Thomas JT, Adamson AJ, Paulson EK. The role of coronal reformations from isotropic voxels using 16-slice MDCT in the diagnosis of small bowel obstruction (abstr). In: Radiological Society of North America scientific assembly and annual meeting program. Oak Brook, Ill: Radiological Society of North America, 2004; 482.